Aluminum Deoxidation Equilibrium of Fe-Ni Alloy at 1773 K and 1873 K

HIROSHI FUKAYA, KOJI KAJIKAWA, ANNELIES MALFLIET, BART BLANPAIN, and MUXING GUO

The aluminum deoxidation equilibrium in molten Fe-36 mass pct Ni and Fe-46 mass pct Ni alloys was experimentally determined at 1773 K and 1873 K to obtain the thermodynamic parameters around the liquidus temperature, which is required to predict the deoxidation reaction for the ingot-casting process. Automatic SEM-EDS inclusion analysis was performed to estimate the undissolved oxygen content. Thermodynamic analysis on Al deoxidation was carried out using Miki and Hino's formula, which is based on Darken's quadratic formalism and the Redlich–Kister polynomial. From the composition dependence of the apparent equilibrium constant in Fe-Ni alloy, the necessity of the third-order interaction parameter of Ni-Al was found. Then, the interaction parameters of Fe-Al, Al-O and Ni-Al were evaluated.

I. INTRODUCTION

TO produce high-quality steel, control of the oxygen content in steel is one of the most important technical issues in the steelmaking process. Due to the strong affinity with oxygen, aluminum is commonly used as a deoxidizing agent in the process. Therefore, since the 1950s many researchers have studied the thermodynamics of aluminum deoxidation in the steel melt.

To describe the Al deoxidation equilibrium in low alloy steel, the first-order interaction parameter formalism of Wagner[1] (Wagner's formula) has been used for practical engineering purposes because of its simple equation and easy application in multicomponent systems. However, since Wagner's formula was inherently derived from the Taylor expansion at infinitely dilute solution, there are many difficulties to applying Wagner's formula to high-alloy steel and steel with high Al levels.

Miki and Hino[2] used Darken's quadratic formalism[3,4] and a Redlich–Kister type polynomial[5,6] to calculate the deoxidation equilibrium in non-dilute alloys. Their formula enables calculating the deoxidation equilibrium in high-alloy steels such as stainless steel.

Even though there have been many studies performed on the Al deoxidation equilibrium in a steel melt, most of these studies were carried out around a typical steel refining temperature (*i.e.*, 1873 K). These studies were intended to describe and/or predict the deoxidation reaction during the steel-refining process.

However, for large ingot casting, the solidification takes a long time. Especially for extremely large ingots, it takes several days to complete the solidification after pouring, which is much longer than the refining time. After pouring the steel melt into the ingot case, the temperature of the steel melt decreases to the liquidus temperature, and then the liquid steel gradually solidifies from the ingot surface to its center. Due to the temperature drop and deoxidizing or oxidizing reactions during casting, the equilibrium state between inclusions and steel melt after pouring might differ from that in the refining process. During the long solidification period, the chemistry of the inclusions in the steel melt might evolve toward the new equilibrium state in the ingot case. Therefore, thermodynamic parameters applicable at solidification temperatures (about 1773 K) are required to describe or predict the deoxidation reactions during solidification for large ingots.

In 2002, Rhee *et al.*[7] carried out an experimental study on the Al deoxidation equilibrium in Fe-36 mass pct Ni alloy at 1773 K using a levitation furnace to obtain the interaction parameters for Wagner's formula. As their parameters were only valid for Al deoxidation in an Fe-36 mass pct Ni alloy at 1773 K, the aim of this study is to extend these data to Fe-Ni alloys with Ni between 36 and 46 mass pct and for temperatures of both 1773 K and 1873 K. Based on the experimentally determined Al deoxidation equilibrium data, the

HIROSHI FUKAYA and KOJI KAJIKAWA are with the Muroran Research Laboratory, The Japan Steel Works, Ltd., Chatsu-machi 4, Muroran, Hokkaido 051-8505, Japan. Contact e-mail: hiroshi_fukaya@jsw.co.jp ANNELIES MALFLIET, BART BLANPAIN, and MUXING GUO are with the Department of Materials Engineering, KU Leuven, Kasteelpark Arenberg 44 - bus 2450, 3000 Louvain, Belgium.

thermodynamics analysis was carried out using Miki and Hino's formula to obtain the thermodynamics parameters applicable for large ingot solidification. Using the parameters determined in this study, the Al deoxidation equilibrium in the complete composition range of Fe-Ni alloys with dilute Al and O at temperatures from 1773 K to 1973 K was calculated.

II. EXPERIMENTS

A. Experimental Setup and Procedure

The experiments were conducted with a vertical heat resistance furnace at purified Ar atmosphere. Figure 1(a) shows a diagram of the experimental setup. The furnace consists of an Al_2O_3 working tube, $MoSi_2$ heating elements, Al_2O_3 gas inlet tube, Al_2O_3 support tube, Al_2O_3 outer protective crucible, Al_2O_3 inner crucible (OD = 24 mm, ID = 20 mm, H = 60 mm), Al_2O_3 brick to fix the inner crucible in the outer crucible and oxygen sensor that measures the oxygen partial pressure at the gas outlet.

The Ar gas was purified by an Mg furnace and silica gel. A feeding chamber was installed at the top of the gas inlet tube, which allows the deoxidizing agent to be added into the crucible without any contamination of the atmosphere. The melt temperature was calibrated by a thermocouple (type S) with Al_2O_3 shielding and controlled within ± 2 °C during experiments.

A. Feeding chamber
B. Deoxidizing agent
C. Rubber stopper
D. Upper flange
E. Working tube
F. Gas inlet tube
G. Al_2O_3 brick
H. Inner crucible
I. Sample
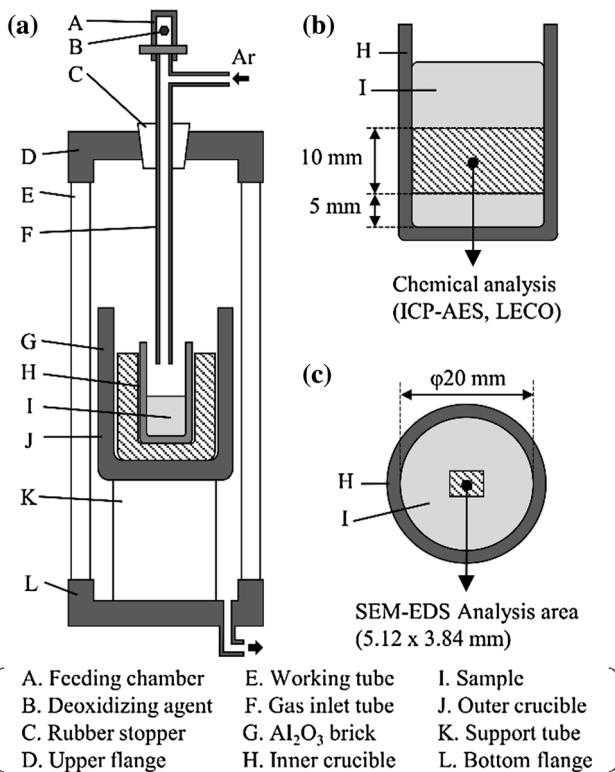J. Outer crucible
K. Support tube
L. Bottom flange

Fig. 1—Schematic diagram of the experimental apparatus and quenched sample: (*a*) experimental apparatus; (*b*) vertical section of the quenched sample; (*c*) horizontal section at 5 mm from the bottom of the sample.

To obtain a homogeneous experimental condition, an Fe-Ni alloy prepared from electrolytic iron (99.99 pct) and nickel (99.99 pct) was used for the deoxidation experiments as a master alloy. About 60 g of the Fe-Ni master alloy was placed in the inner crucible and set into the furnace. After the gas atmosphere was changed to the purified Ar, the Fe-Ni alloy was heated and melted completely at 1873 K. High-purity Al grain (0.03 to 0.12 g) as a deoxidizing agent was added to the melt from the feeding chamber through the gas inlet tube. The melt was then stirred with an Al_2O_3 rod for 1 min. The temperature was controlled at the temperature of interest (1773 K, 1873 K) for more than 8 hours. A holding time of 8 hours was considered sufficient to reach equilibrium based on preliminary experiments. Then, the melt with the inner crucible was picked up from the furnace and rapidly water quenched.

B. Chemical Analysis of Metal and Characterization of Inclusion

The quenched samples were analyzed by the following techniques. Figure 1(b) and (c) shows a diagram of the extraction of the quenched sample for steel composition analysis (ICP-AES, LECO) and SEM-EDS inclusion characterization. Ni and Al contents were analyzed using inductively coupled plasma optical emission spectroscopy (Varian 720ES, Agilent Technology Co). Sample solutions for Ni measurement were prepared by dissolving 1.0 g metal sample in HNO_3 (1:1) and filling the 100-ml flask with deionized water. Sample solutions for Al measurement were obtained by diluting the Ni measurement solutions to 1/100. Because the concentrations of Fe and Ni in the sample solutions were much higher than those of Al, the Al spectrum might be affected by Fe and Ni. To minimize the effect of Fe and Ni as background elements in the sample solutions, standard solutions containing the same amount of Fe and Ni were used for Al measurement. The total O content was analyzed by using inert gas infrared fusion spectroscopy (TC-436, LECO Co). Each specimen was cleaned by using ultrasonic cleaning in methanol after grinding by SiC abrasive paper. Each sample was analyzed at least three times to confirm the reliability of the analysis. The Fe content was obtained as the residue of the Ni, Al and O contents.

SEM-EDS (JSM-6610LA, JEOL Co, Japan) and Particle Finder (JEOL ENGINEERING Co, Japan) were employed for the inclusion analysis. Horizontal cross sections of the Fe-Ni samples 5 mm from the bottom of the crucible were cut, ground by SiC abrasive paper and polished prior to the inclusion characterization by SEM-EDS with Particle Finder. As shown in Figure 1(c), an area of 19.66 mm^2 was scanned, and backscattered electron (BSE) images were recorded. The precision of the results by taking an area of 19.66 mm^2 was verified by measuring six fields of 19.66 mm^2 in serial sections in two samples (nos. 3 and 5). The deviation of the inclusion area fraction was smaller than 10 pct from the average. Due to the difference in average atomic number between the metal matrix phase and oxide inclusions, all inclusions > 0.1 μm^2 were

automatically detected by the contrast in the BSE image. The chemical compositions of the detected inclusions were simultaneously analyzed by EDS. Since the inclusion sizes were very small, the results of EDS analysis might be affected by the Fe-Ni metallic matrix phase. To eliminate this background effect, peaks of Fe and Ni in EDS spectra were ignored in the quantitative composition analysis of inclusions. Using this technique, information about all detected inclusions such as size, shape, distribution and composition was obtained. For example, the BSE image and EDS spectrum of one of the detected inclusions in sample no. 1 is shown in Figure 2. Almost all detected inclusions in this study have a spherical or angular shape and are not clustered. The boundary of the particle was not sharp. The width of the uncertainness boundary was 0.15 μm. This might influence the estimation of the undissolved oxygen content (see Section III–A). Considering that half of the uncertainness boundary width causes an error in inclusion size measurement, the error was estimated to be 30 pct in the case of the average inclusion size (1.87 μm^2). Although this value was not small, most of the undissolved oxygen contents in this experiment were smaller than the total oxygen contents. Therefore, the error in the inclusion size measurement will not cause significant results.

III. RESULTS AND DISCUSSION

A. Methodology to Evaluate the Dissolved and Undissolved Oxygen

One of the possible reasons for the large deviation in the Al-O relation in previous studies on the Al deoxidation equilibrium is the influence of oxide inclusions on the oxygen analysis (i.e., the undissolved oxygen). A reliable analysis of the dissolved oxygen content is required for the determination of the deoxidation equilibrium. However, if the metal sample for the oxygen analysis contains some oxide inclusions, the results of Al-O equilibrium will be affected by the oxygen in these inclusions. Especially for

experiments conducted in a heat resistance furnace, the force to separate inclusions from the melt is smaller than in an induction furnace, as the latter has a pinch effect, which ejects inclusions from the melt. In spite of the long holding time, some inclusions might remain in the metal phase, specifically the tiny inclusions. In this study, the results of the inert gas infrared fusion spectroscopy (LECO) are assumed to be the total oxygen content (O_{Tot}), expressed in Eq. [1].

$$O_{Tot} = O_D + O_U \qquad [1]$$

where O_D and O_U mean respectively the dissolved oxygen content in the metal phase and the oxygen content in the inclusions. The oxygen content in the inclusions O_U was determined by measuring the size and composition of all inclusions using SEM-EDS. The average composition of the inclusions detected by SEM-EDS is shown in Table I. Although SiO$_2$, MgO, CaO and ZrO$_2$ were detected as minor oxides, the average composition of Al$_2$O$_3$ was more than 97 pct. No sulfide or any other compounds were observed in the inclusions. Al$_2$O$_3$ is therefore the dominant oxide in this work, and the activity of Al$_2$O$_3$ can be considered as unity.

When the inclusion particles are distributed randomly, the area fraction of the particles in an arbitrary section is equal to the volume fraction of the particles.[8] Since the volume fraction of the inclusions was very small, the oxygen content of the inclusions can be calculated by Eq. [2]:

$$\begin{aligned}
O_U &= \frac{\rho_{Al_2O_3} \sum S_{Inclusion}}{\rho_{Fe-Ni}(S_{Total} - \sum S_{Inclusion}) + \rho_{Al_2O_3} \sum S_{Inclusion}} \\
&\quad \times \left(\frac{3M_O}{M_{Al_2O_3}}\right) \times 100 \\
&= \frac{\rho_{Al_2O_3} \sum S_{Inclusion}}{\rho_{Fe-Ni} S_{Total}} \left(\frac{3M_O}{M_{Al_2O_3}}\right) \\
&\quad \times 100 \left(\because \sum S_{Inclusion} \ll S_{Total}\right)
\end{aligned}$$
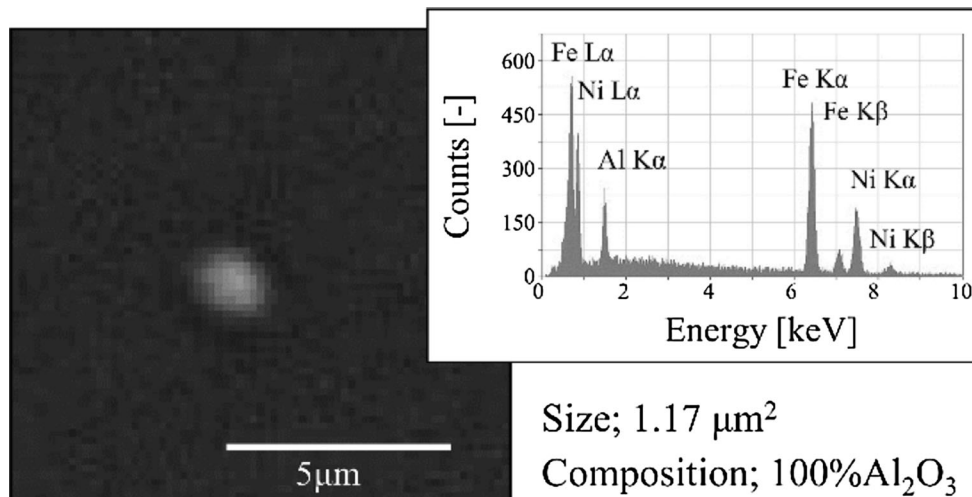
$$[2]$$

Size; 1.17 μm^2
Composition; 100%Al$_2$O$_3$

Fig. 2—Example of the determination of the particle size from the BSE image and the EDS analysis (sample no. 1).

where ρ_i, $\sum S_{Inclusion}$, S_{Total} and M_i are respectively the density of component i, the sum of the inclusions area, the total investigated area (19.66 mm^2) and the molecular and/or atomic weight of component i. O_D is then obtained by combining Eqs. [1] and [2].

B. Experimental Results

Table II shows the results of the ICP-AES, total oxygen and the SEM-EDS inclusion analysis. Figure 3 shows the Al-O relation of this work. For comparison, the results of the previous studies[7,9–11] are also plotted in the figure on Al deoxidation in Fe-36 and 46 mass pct Ni alloy at 1773 K to 1973 K. The area fraction of the inclusions is proportional to the undissolved oxygen content (Table II). Although the undissolved oxygen content was mostly lower than 1 ppm, a maximum of 5.2 ppm was found. The effect of the undissolved oxygen content is not negligible in the high Al range and at lower temperature to calculate the deoxidation equilibrium and/or to determine the thermodynamic parameters, as the dissolved O content has the same order of magnitude as the O content in the inclusions. This may

explain the deviation between the present study and the investigation by Rhee et al.[7] In the low Al range (< 0.5 mass pct Al), the present results for Fe-36 mass pct Ni at 1773 K are in a good accordance with Rhee's results, except for the data point with the lowest Al content (no. 1). However, in the high Al range (> 0.5 mass pct Al), the equilibrated oxygen contents in the present work are smaller than those in Rhee's experiment. This indicates that the determination of the oxygen content in the inclusions by using SEM-EDS inclusion analysis enables obtaining more accurate equilibrium data for the high Al content steel. The dissolved oxygen contents in the metal matrix phase are used for the numerical analysis in this study.
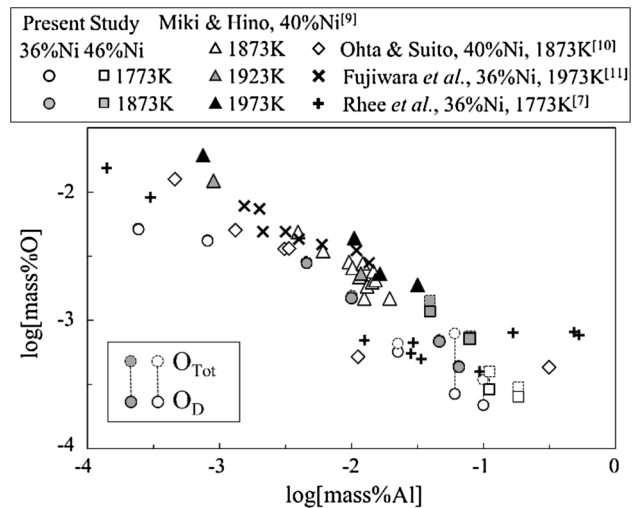
C. Al Deoxidation Equilibrium in Fe-Ni Alloys

1. Thermodynamic description of the Al deoxidation

In this study, the Redlich–Kister type polynomial proposed by Miki and Hino[2] was used for the thermodynamic analysis of the Al deoxidation equilibrium. The pure substance was chosen as the standard

Table I. Average Composition of the Detected Inclusions by Auto SEM-EDS Analysis

| No.	Average Composition [Mass Pct]				
	MgO	Al$_2$O$_3$	SiO$_2$	CaO	ZrO$_2$
1	0.9	99.1	0	0	0
2	0.2	99.4	0.4	0	0
3	1.2	97.9	0.8	0.1	0
4	0.7	99.2	0.1	0	0
5	0.5	99.5	0	0	0
6	0.6	99.4	0	0	0
7	1.3	98.7	0	0	0
8	0	100	0	0	0
9	1.4	98.6	0	0	0
10	1.2	97.0	0.7	1.1	0
11	0	97.2	0.5	0.8	1.5
12	0	99.9	0.1	0	0
13	0.1	98.4	0	0	1.4

Fig. 3—Experimental results and Al deoxidation equilibrium in Fe-36 to 46 pct Ni.

Table II. Experimental Results

No.	Temp. [K]	Ni [Mass Pct]	Al [ppm]	O$_{Tot}$ [ppm]	O$_U$ [ppm]	O$_D$ [ppm]	Number Density [-/mm^2]	Inclusion Area Fraction $\sum S_{Inclusion}/S_{Total}$ [μm^2/mm^2]
1	1773	37.3	2.4	51.7	0.5	51.2	0.4	2.2
2	1773	36.6	8.1	41.9	0.3	41.6	1.0	1.6
3	1773	37.1	224	6.6	0.9	5.7	2.0	4.1
4	1773	36.6	605	7.9	5.2	2.7	6.9	22.7
5	1773	36.6	996	3.45	1.3	2.2	1.6	5.5
6	1773	45.4	1108	4.0	1.1	2.9	3.7	4.8
7	1773	45.7	1833	3.0	0.5	2.5	0.7	2.0
8	1873	36.6	45.6	28.5	0.7	27.8	3.9	2.8
9	1873	36.8	101	15.6	0.7	14.8	1.3	3.2
10	1873	36.3	463	7.0	0.1	6.9	0.2	0.7
11	1873	36.1	649	4.4	0.0	4.4	0.2	0.2
12	1873	45.8	393	14.2	2.4	11.8	10.3	10.4
13	1873	45.5	791	7.5	0.3	7.2	0.7	1.3

state for the condensed phases (Fe, Ni and Al). Dissolved oxygen equilibrated with 1 atm (0.1 MPa) oxygen was used as the standard state for oxygen. The Al deoxidation reaction can be expressed as Eq. [3]:

$$2Al(l) + 3\underline{O} = Al_2O_3(s) \qquad [3]$$
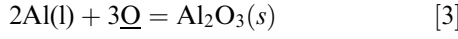
For the selected standard state for oxygen, the Gibbs free energy change of Eq. [3] is equal to the Gibbs free energy of Al_2O_3 formation ($\Delta G^{\circ}_{f.Al_2O_3}$). Therefore, the equilibrium constant K of Eq. [3] is described as Eq. [4]:

$$\begin{aligned}
\ln K &= -\frac{\Delta G^{\circ}_{f.Al_2O_3}}{RT} \\
&= \ln a_{Al_2O_3} - 2\ln a_{Al} - 3\ln a_O \\
&= -2\ln \gamma_{Al} X_{Al} - 3\ln \gamma_O X_O (\because a_{Al_2O_3} = 1) \\
&= -2\ln X_{Al} - 2\ln \gamma_{Al} - 3\ln X_O - 3\ln \gamma_O
\end{aligned} \qquad [4]$$

where a_i, γ_i and X_i are respectively the activity, activity coefficient and molar fraction of component i. The excess free energy change of the Fe-Ni-Al-O system (ΔG^{ex}) can be expressed as a Redlich–Kister type polynomial using the first- and second-order interactions (Eq. [5]). Here, since the mole fractions of Al and O are small enough, only the first-order interaction parameter on Al and O is considered.

$$\begin{aligned}
\Delta G^{ex} &= X_{Fe}X_{Ni}\{{}^0\Omega_{Fe-Ni} + (X_{Fe} - X_{Ni})^1\Omega_{Fe-Ni}\} \\
&+ X_{Fe}X_{Al}\{{}^0\Omega_{Fe-Al} + (X_{Fe} - X_{Al})^1\Omega_{Fe-Al}\} \\
&+ X_{Fe}X_O\{{}^0\Omega_{Fe-O} + (X_{Fe} - X_O)^1\Omega_{Fe-O}\} \\
&+ X_{Ni}X_{Al}\{{}^0\Omega_{Ni-Al} + (X_{Ni} - X_{Al})^1\Omega_{Ni-Al}\} \\
&+ X_{Ni}X_O\{{}^0\Omega_{Ni-O} + (X_{Ni} - X_O)^1\Omega_{Ni-O}\} \\
&+ X_{Al}X_O{}^0\Omega_{Al-O}
\end{aligned} \qquad [5]$$

Here, ${}^0\Omega_{i-j}$ and ${}^1\Omega_{i-j}$ are respectively the first- and second-order interaction parameters between component i and j. The partial molar excess free-energy changes of Al and O can by expressed by Eqs. [6] and [7]:

$$\begin{aligned}
\Delta \overline{G}^{ex}_{Al} &= RT\ln \gamma_{Al} \\
&= \Delta \overline{G}^{ex} - X_{Ni}\frac{\partial \Delta \overline{G}^{ex}}{\partial X_{Ni}} \\
&+ (1 - X_{Al})\frac{\partial \Delta \overline{G}^{ex}}{\partial X_{Al}} - X_O\frac{\partial \Delta \overline{G}^{ex}}{\partial X_O} \\
&= -X_{Fe}X_{Ni}{}^0\Omega_{Fe-Ni} - 2X_{Fe}X_{Ni}(X_{Fe} - X_{Ni})^1\Omega_{Fe-Ni} \\
&+ X_{Fe}(1 - X_{Al})^0\Omega_{Fe-Al} \\
&+ X_{Fe}(X_{Fe} - 2X_{Al} - 2X_{Fe}X_{Al} + 2X_{Al}^2)^1\Omega_{Fe-Al} \\
&- X_{Fe}X_O{}^0\Omega_{Fe-O} - 2X_{Fe}X_O(X_{Fe} - X_O)^1\Omega_{Fe-O} \\
&+ X_{Ni}(1 - X_{Al})^0\Omega_{Ni-Al} \\
&+ X_{Ni}(X_{Ni} - 2X_{Al} - 2X_{Ni}X_{Al} - 2X_{Al}^2)^1\Omega_{Ni-Al} \\
&- X_{Ni}X_O{}^0\Omega_{Ni-O} - 2X_{Ni}X_O(X_{Ni} - X_O)^1\Omega_{Ni-O} \\
&+ X_O(1 - X_{Al})^0\Omega_{Al-O}
\end{aligned} \qquad [6]$$

$$\begin{aligned}
\Delta \overline{G}^{ex}_O &= RT\ln \gamma_O \\
&= \Delta \overline{G}^{ex} - X_{Ni}\frac{\partial \Delta \overline{G}^{ex}}{\partial X_{Ni}} + (1 - X_O)\frac{\partial \Delta \overline{G}^{ex}}{\partial X_O} - X_{Al}\frac{\partial \Delta \overline{G}^{ex}}{\partial X_{Al}} \\
&= -X_{Fe}X_{Ni}{}^0\Omega_{Fe-Ni} - 2X_{Fe}X_{Ni}(X_{Fe} - X_{Ni})^1\Omega_{Fe-Ni} \\
&- X_{Fe}X_{Al}{}^0\Omega_{Fe-Al} - 2X_{Fe}X_{Al}(X_{Fe} - X_{Al})^1\Omega_{Fe-Al} \\
&+ X_{Fe}(1 - X_O)^0\Omega_{Fe-O} \\
&+ X_{Fe}(X_{Fe} - 2X_O - 2X_{Fe}X_O + 2X_O^2)^1\Omega_{Fe-O} \\
&- X_{Ni}X_{Al}{}^0\Omega_{Ni-Al} - 2X_{Ni}X_{Al}(X_{Ni} - X_{Al})^1\Omega_{Ni-Al} \\
&+ X_{Ni}(1 - X_O)^0\Omega_{Ni-O} \\
&+ X_{Ni}(X_{Ni} - 2X_O - 2X_{Ni}X_O - 2X_O^2)^1\Omega_{Ni-O} \\
&+ X_{Al}(1 - X_O)^0\Omega_{Al-O}
\end{aligned} \qquad [7]$$

By substituting Eqs. [6] and [7] into Eq. [4], the fundamental equation for the thermodynamic analysis of Al deoxidation in Fe-Ni alloy is obtained (Eq. [8])[9]:

$$\begin{aligned}
0 &= 2RT\ln X_{Al} + 3RT\ln X_O - \Delta G^{\circ}_{f.Al_2O_3} \\
&- 5X_{Fe}X_{Ni}{}^0\Omega_{Fe-Ni} - 10X_{Fe}X_{Ni}(X_{Fe} - X_{Ni})^1\Omega_{Fe-Ni} \\
&+ X_{Fe}(2 - 5X_{Al})^0\Omega_{Fe-Al} + X_{Fe}(2X_{Fe} - 4X_{Al} \\
&- 10X_{Fe}X_{Al} + 10X_{Al}^2)^1\Omega_{Fe-Al} + X_{Fe}(3 - 5X_O)^0\Omega_{Fe-O} \\
&+ X_{Fe}(3X_{Fe} - 6X_O - 10X_{Fe}X_O + 10X_O^2)^1\Omega_{Fe-O} \\
&+ X_{Ni}(2 - 5X_{Al})^0\Omega_{Ni-Al} + X_{Ni}(2X_{Ni} - 4X_{Al} \\
&- 10X_{Ni}X_{Al} + 10X_{Al}^2)^1\Omega_{Ni-Al} + X_{Ni}(3 - 5X_O)^0\Omega_{Ni-O} \\
&+ X_{Ni}(3X_{Ni} - 6X_O - 10X_{Ni}X_O - 10X_O^2)^1\Omega_{Ni-O} \\
&+ (3X_{Al} + 2X_O - 5X_{Al}X_O)^0\Omega_{Al-O}
\end{aligned} \qquad [8]$$

All parameters in Eq. [8] were proposed by Miki and Hino.[9] To evaluate the validity of their parameters, the calculated correlation between Al and O is shown in Figures 4 (Fe) and 5 (Ni).

Figure 4 shows the Al deoxidation equilibrium in Fe at 1873 K.[9,12–24] The Al-O curve of the present study (see the discussion in Section III–C–2) is obtained by using Miki and Hino's formula,[9] whereas JSPS[23] and Itoh et al.[24] applied Wagner's formulas and Paek et al.[21,22] used the Modified Quasichemical Model (MQM model). In the high Al region (Al > 1.0 mass pct) all calculated curves except the one of Paek et al.[21,22] deviate from the experimental data. Pelton et al.[25] and Paek et al.[21,22] explained that, due to the strong affinity between Al and O, the regular solution model (random mixing of components), which has been assumed for Miki and Hino's[9] formula, does not apply there. However, except for special high Al-containing steels, this deviation in the high Al range is rarely a problem in the practical engineering of the steel production. Although applying the MQM model as done by Paek et al.[21,22] gives a good agreement between
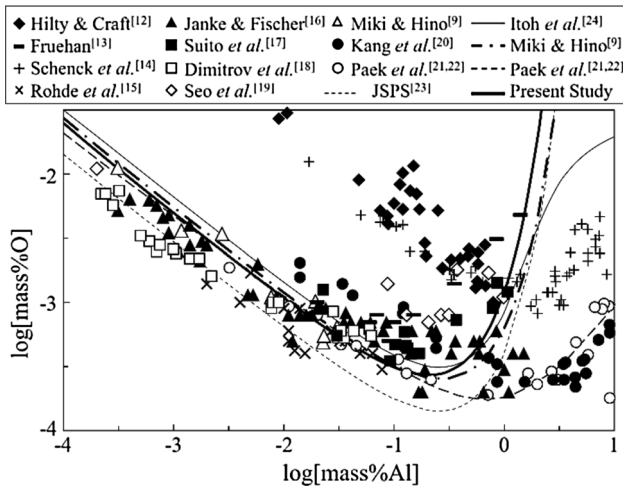
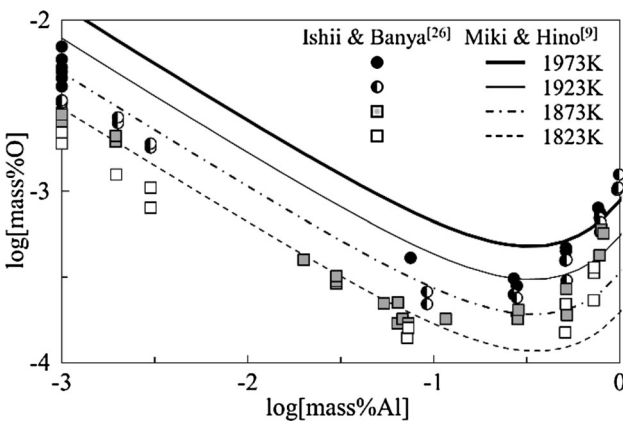Fig. 4—Al deoxidation equilibrium in Fe at 1873 K.

Fig. 5—Al deoxidation equilibrium in Ni at 1823 K to 1973 K.

calculation and experimental data in the high Al region, the application of the Al deoxidation in multicomponent systems has not been examined yet. On the other hand, despite the deviation in the high Al region, Miki and Hino's [9] calculation is in a good agreement with that of other researchers except for the results of Hilty and Crafts[12] and Schenck et al.[14] in the low Al region (Al < 0.5 mass pct). Itoh et al.[24] considered that the deviations in these two studies[12,14] were generated from uncertainties of temperature and oxygen measurements.

Figure 5 shows the Al-O correlation of the Al deoxidation equilibrium in Ni at 1823 K to 1973 K in which the calculated curve using Miki and Hino's parameters[9] is compared with the experimental data by Ishii and Banya.[26] It is clear that the calculated curve does not agree with the experimental data.[26] This indicates that the parameters proposed by Miki and Hino[9] need to be modified to satisfy the experimental results in the full composition range of Fe-Ni alloys. To identify which parameters need modification, the

reliability of the applied interaction parameters by Miki and Hino was checked; $\Delta G^\circ_{f,Al_2O_3}$ was taken from NIST-JANAF Thermochemical Tables.[27] The Fe-Ni interaction parameters ($^0\Omega_{Fe-Ni}$ and $^1\Omega_{Fe-Ni}$) were taken from the Fe-Ni binary phase diagram.[28] The interaction parameters of Fe-O ($^0\Omega_{Fe-O}$ and $^1\Omega_{Fe-O}$) and Ni-O ($^0\Omega_{Ni-O}$ and $^1\Omega_{Ni-O}$) were obtained from the Gibbs free energy change of oxygen dissolution into molten Fe[23] and Ni[28] and the self-interaction coefficient of oxygen in molten Fe[23] and Ni.[28] The interaction parameters of Fe-Ni, Fe-O and Ni-O were also used in the study of Si deoxidation in Fe, Ni, Fe-Ni, Fe-Cr, Fe-Cr-Ni, Ni-Cu and Ni-Co alloys,[2,29] and their validity for the calculations was confirmed. On the other hand, the interaction parameters around Al (*i.e.*, Fe-Al, Ni-Al and Al-O interactions) were obtained only from the Fe and Fe-Ni alloy. Since the calculation in Ni does not fit well with the experimental data (Figure 5), interaction parameters around Al should be less reliable than the other interaction parameters. There are also mathematical difficulties in the parameter determination in Miki and Hino[9]; for example, for $^0\Omega_{Ni-Al}$ and $^1\Omega_{Ni-Al}$ determination, Eq. [8] was converted into Eq. [9],

$$
\begin{aligned}
&- \{ -5X_{Fe}X_{Ni}{}^0\Omega_{Fe-Ni} - 10X_{Fe}X_{Ni}(X_{Fe} - X_{Ni})^1\Omega_{Fe-Ni} \\
&+ X_{Fe}(2 - 5X_{Al})^0\Omega_{Fe-Al} + X_{Fe}(2X_{Fe} - 4X_{Al} \\
&- 10X_{Fe}X_{Al} + 10X_{Al}^2)^1\Omega_{Fe-Al} + X_{Fe}(3 - 5X_O)^0\Omega_{Fe-O} \\
&+ X_{Fe}(3X_{Fe} - 6X_O - 10X_{Fe}X_O + 10X_O^2)^1\Omega_{Fe-O} \\
&+ X_{Ni}(3 - 5X_O)^0\Omega_{Ni-O} + X_{Ni}(3X_{Ni} - 6X_O - 10X_{Ni}X_O \\
&- 10X_O^2)^1\Omega_{Ni-O} + (3X_{Al} + 2X_O - 5X_{Al}X_O)^0\Omega_{Al-O} \\
&+ 2RT\ln X_{Al} + 3RT\ln X_O - \Delta G^\circ_{Al_2O_3} \} / X_{Ni}(2 - 5X_{Al}) \\
&= {}^0\Omega_{Ni-Al} + \frac{(2X_{Ni} - 4X_{Al} - 10X_{Ni}X_{Al} + 10X_{Al}^2)}{(2 - 5X_{Al})}{}^1\Omega_{Ni-Al}
\end{aligned}
$$

[9]

By defining the left side of Eq. [9] as Y_{Ni-Al} and the coefficient term of $^1\Omega_{Ni-Al}$ as X_{Ni-Al}, Eq. [9] can be simplified to Eq. [10].

$$ Y_{Ni-Al} = {}^0\Omega_{Ni-Al} + X_{Ni-Al}{}^1\Omega_{Ni-Al} \qquad [10] $$

Then, using experimental data and known parameters and taking Y_{Ni-Al} as a vertical axis and X_{Ni-Al} as a horizontal axis, $^0\Omega_{Ni-Al}$ and $^1\Omega_{Ni-Al}$ can be determined, respectively, as the intercept and the slope of the regression line. Since X_{Ni-Al} is approximately equal to X_{Ni} in the low Al content range, $^0\Omega_{Ni-Al}$ means a value of Y_{Ni-Al} at Fe ($X_{Ni} = 0$). Since Y_{Ni-Al} contains a term with the inverse of X_{Ni} (see Eq. [9]), a small error in experimental data will result in a large deviation in Y_{Ni-Al} at the low X_{Ni} region ($X_{Ni} \rightarrow 0$). Therefore, it is difficult to mathematically obtain reliable parameters in this way. In addition, this linear regression method cannot be applied for the

determination of higher order interaction parameters. This is because with higher order interaction parameters it cannot be expressed by a linear line anymore. Therefore, modified interaction parameters of Fe-Al, Ni-Al and Al-O for a correct description of the Al deoxidation of Fe-Ni alloy during solidification for large ingots are proposed in the next section.

2. *Determination of Fe-Al, Ni-Al and Al-O interaction parameters*

In the present study, the interaction parameters of the Al deoxidation equilibrium were determined from the apparent equilibrium constant ($\log K'$) in Fe-Ni alloys. It is well known that the deoxidation reaction product of the Al deoxidation equilibrium is a constant value at low Al content range (Al < 0.5 mass pct), where there is a linear relation between Al and O contents and the apparent deoxidation constant is a function of temperature and alloy composition.

Figure 6 shows the apparent equilibrium constant ($\log K'$) of the Al deoxidation equilibrium in Fe-Ni alloy,[7,9–11,26,30] where the apparent equilibrium constant in Fe ($\log K'_{Fe}$) and that in Ni ($\log K'_{Ni}$) are adopted from the work of Seo *et al.*[24] and Ishii *et al.*[26]

$$\log K'_{Fe} = 12.32 - 47400/T \qquad [11]$$

$$\log K'_{Ni} = 1.67 - 28770/T \qquad [12]$$

By fitting the apparent equilibrium constants for Fe and Ni, respectively, through Eqs. [11] and [12] with the ones calculated from experimental data for Fe-Ni alloys, the $\log K'$ in the full range of Fe-Ni alloy from 1773 K to 1973 K is estimated as the dotted lines in Figure 6. There is a maximum $\log K'$ value around 50 to 60 mass pct Ni at each of the equilibrium temperatures. Although deoxidation products are gradually increasing with Ni content in the lower Ni region, it drops around 80 mass pct Ni.

Since X_{Al} and X_O are small enough in the region where the Al and O content have a linear relation, the standard equation of the Al deoxidation equilibrium in the Fe-Ni-Al-O system (Eq. [8]) can be simplified to Eq. [13] by eliminating X_{Al} and X_O and by replacing X_{Fe} by ($1-X_{Ni}$).

$$
\begin{aligned}
RT &\ln X_{Al}^2 \cdot X_O^3 - \Delta G^\circ_{f.Al_2O_3} - 5(1 - X_{Ni})X_{Ni}{}^0\Omega_{Fe-Ni} \\
&- 10X_{Ni}(1 - X_{Ni})(1 - 2X_{Ni}){}^1\Omega_{Fe-Ni} \\
&= -2(1 - X_{Ni}){}^0\Omega_{Fe-Al} - 2(1 - X_{Ni})^2{}^1\Omega_{Fe-Al} \\
&- 3(1 - X_{Ni}){}^0\Omega_{Fe-O} - 3(1 - X_{Ni})^2{}^1\Omega_{Fe-O} \\
&- 2X_{Ni}{}^0\Omega_{Ni-Al} - 2X_{Ni}^2{}^1\Omega_{Ni-Al} - 3X_{Ni}{}^0\Omega_{Ni-O} \\
&- 3X_{Ni}^2{}^1\Omega_{Ni-O}
\end{aligned}
\qquad [13]
$$

The deoxidation product in mole fraction ($\ln X_{Al}^2 X_O^{3-}$) can be expressed by Eq. [14] using $\log K'$ in the low Al and O content region:
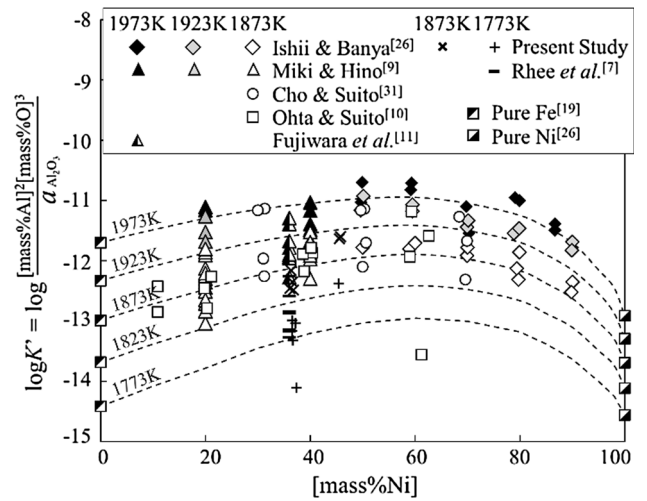

Fig. 6—Apparent equilibrium constant ($\log K'$) of Al deoxidation in Fe-Ni alloy.

$$
\begin{aligned}
&\ln X_{Al}^2 \cdot X_O^3 \\
&= \ln\left(\frac{\left(\frac{[pct\ Al]}{M_{Al}}\right)^2\left(\frac{[pct\ O]}{M_O}\right)^3}{\left(\frac{100 - [pct\ Ni] - [pct\ Al] - [pct\ O]}{M_{Fe}} + \frac{[pct\ Ni]}{M_{Ni}} + \frac{[pct\ Al]}{M_{Al}} + \frac{[pct\ O]}{M_O}\right)^5}\right) \\
&= \ln\frac{[pct\ Al]^2[pct\ O]^3}{M_{Al}^2 M_O^3} - 5\ln\left(\frac{100 - [pct\ Ni]}{M_{Fe}} + \frac{[pct\ Ni]}{M_{Ni}}\right) \\
&\quad (\because [pct\ Al],\ [pct\ O] \ll 1) \\
&= 2.303\log K' - \ln M_{Al}^2 \cdot M_O^3 - 5\ln\left(\frac{100 - [pct\ Ni]}{M_{Fe}} + \frac{[pct\ Ni]}{M_{Ni}}\right)
\end{aligned}
\qquad [14]
$$

Defining the left side of Eq. [13] as F, -F consists then of $\log K'$, Ni content, temperature and known parameters ($\Delta G^\circ_{f.Al_2O_3}$, $^0\Omega_{Fe-Ni}$ and $^1\Omega_{Fe-Ni}$). Figure 7 shows a plot of the left side of Eq. [13] (*i.e.*, F) against X_{Ni}, using the estimated values of $\log K'$ for Fe-Ni alloy at 1773 K to 1973 K from Figure 6 together with the calculated curves by using Miki and Hino's parameters[9] and using the parameters determined in this study. This asymmetry in the F curves resembles the asymmetry in the $\log K'$ curves. However, the right side of Eq. [13], which consists of X_{Ni} and first- and second-order interaction parameters (Fe-Al, Fe-O, Ni-Al and Ni-O), is a quadratic function with X_{Ni} as a variable. As asymmetric curves for F cannot be expressed by a quadric function of X_{Ni}, the curves calculated by the Miki and Hino's parameters, which contain the second-order interaction parameters,[9] did not correspond with the curves estimated from $\log K'$. Therefore, to describe the asymmetric F curves estimated from $\log K'$, the higher order interaction parameter was introduced in this study.

As mentioned in Section III–C–1, the interaction parameters of Fe-O and Ni-O were confirmed to be reliable to describe the Si deoxidation in many systems.[2,29] Because the F-X_{Ni} relation (see Figure 7) greatly changes in the high Ni region, where the Ni-Al interaction is stronger than the Fe-Al interaction, the third-order Ni-Al interaction is considered in the present
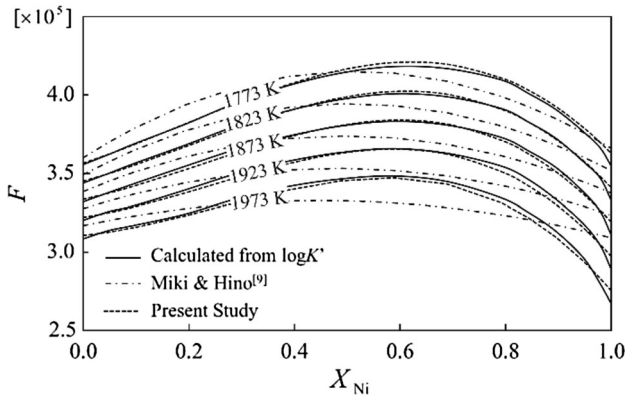
Fig. 7—F curves against X_{Ni} at 1773 K to 1973 K.

study. By introducing the third-order Ni-Al interaction parameter ($^2\Omega_{Ni-Al}$), Eqs. [8] and [13] are changed into Eqs. [15] and [16], respectively.

$$
\begin{aligned}
&- 5X_{Fe}X_{Ni}{}^0\Omega_{Fe-Ni} - 10X_{Fe}X_{Ni}(X_{Fe} - X_{Ni})^1\Omega_{Fe-Ni} \\
&+ X_{Fe}(2 - 5X_{Al})^0\Omega_{Fe-Al} + X_{Fe}(2X_{Fe} - 4X_{Al} \\
&- 10X_{Fe}X_{Al} + 10X_{Al}^2)^1\Omega_{Fe-Al} + X_{Fe}(3 - 5X_O)^0\Omega_{Fe-O} \\
&+ X_{Fe}(3X_{Fe} - 6X_O - 10X_{Fe}X_O + 10X_O^2)^1\Omega_{Fe-O} \\
&+ X_{Ni}(2 - 5X_{Al})^0\Omega_{Ni-Al} + X_{Ni}(2X_{Ni} - 4X_{Al} \\
&- 10X_{Ni}X_{Al} + 10X_{Al}^2)^1\Omega_{Ni-Al} + X_{Ni}(X_{Ni} - X_{Al}) \\
&\times (2X_{Ni} - 6X_{Al} - 15X_{Ni}X_{Al} + 15X_{Al}^2)^2\Omega_{Ni-Al} \\
&+ X_{Ni}(3 - 5X_O)^0\Omega_{Ni-O} + X_{Ni}(3X_{Ni} - 6X_O \\
&- 10X_{Ni}X_O - 10X_O^2)^1\Omega_{Ni-O} + (3X_{Al} + 2X_O \\
&- 5X_{Al}X_O)^0\Omega_{Al-O} + 2RT\ln X_{Al} + 3RT\ln X_O \\
&- \Delta G^\circ_{f.Al_2O_3} = 0
\end{aligned} \tag{15}
$$

$$
\begin{aligned}
F = &-2(1 - X_{Ni})^0\Omega_{Fe-Al} - 2(1 - X_{Ni})^{2\,1}\Omega_{Fe-Al} \\
&- 3(1 - X_{Ni})^0\Omega_{Fe-O} - 3(1 - X_{Ni})^{2\,1}\Omega_{Fe-O} \\
&- 2X_{Ni}{}^0\Omega_{Ni-Al} - 2X_{Ni}^2{}^1\Omega_{Ni-Al} - 2X_{Ni}^3{}^2\Omega_{Ni-Al} \\
&- 3X_{Ni}{}^0\Omega_{Ni-O} - 3X_{Ni}^2{}^1\Omega_{Ni-O}
\end{aligned} \tag{16}
$$

Equation [15] is the fundamental equation for the numerical analysis of Al deoxidation in Fe-Ni alloy taking into account the third-order interaction parameter of Ni-Al. From Eq. [16], at $X_{Ni} = 0$, where the Ni-Al interaction terms are equal to zero, the Fe-Al interaction parameters can be obtained as:

$$
^0\Omega_{Fe-Al} = -291670 + 117.4T \tag{17}
$$

$$
^1\Omega_{Fe-Al} = 85260 - 39.36T \tag{18}
$$

By fitting the curves in Figure 7 with a cubic function, F can be expressed as Eq. [19]:

$$
F = aX_{Ni}^3 + bX_{Ni}^2 + cX_{Ni} + d \tag{19}
$$

where, a, b, c and d are obtained respectively as Eqs. [20] through [23]

$$
a = -2^2\Omega_{Ni-Al} \tag{20}
$$

$$
b = -2^1\Omega_{Fe-Al} - 3^1\Omega_{Fe-O} - 2^1\Omega_{Ni-Al} - 3^1\Omega_{Ni-O} \tag{21}
$$

$$
\begin{aligned}
c = &2^0\Omega_{Fe-Al} + 4^1\Omega_{Fe-Al} + 3^0\Omega_{Fe-O} + 6^1\Omega_{Fe-O} \\
&- 2^1\Omega_{Ni-Al} - 3^1\Omega_{Ni-O}
\end{aligned} \tag{22}
$$

$$
d = -2(^0\Omega_{Fe-Al} + {}^1\Omega_{Fe-Al}) - 3(^0\Omega_{Fe-O} + {}^1\Omega_{Fe-O}) \tag{23}
$$

From Eqs. [20] through [23], the Ni-Al interaction parameters were determined to be:

$$
^0\Omega_{Ni-Al} = -97200 + 30.0T \tag{24}
$$

$$
^1\Omega_{Ni-Al} = -301800 + 40.5T \tag{25}
$$

$$
^2\Omega_{Ni-Al} = -62900 + 104.5T \tag{26}
$$

By using above new parameter, the mixing enthalpy of Ni-Al binary alloy at $X_{Ni} = 0.5$ was -24 kJ/mol. This value was comparable with the estimated value (-22 kJ/mol) by Niessen et al.[31] The value of calculated γ°_{Al} ($RT\ln\gamma^\circ_{Al} = {}^0\Omega_{Ni-Al} + {}^1\Omega_{Ni-Al} + {}^2\Omega_{Ni-Al}$) in molten Ni at 1873 K was 0.00018. It was also comparable with the values reported by Ishii et al. (0.00022),[26] Sigworth et al. (0.0002)[32] and Dyubanov el al. (0.00016).[33]

Moreover, by rearranging Eq. [15], the first-order interaction parameter of Al-O can be determined through Eq. [27]:

$$
\begin{aligned}
Y_{Al-O} = &2RT\ln X_{Al} + 3RT\ln X_O - \Delta G^\circ_{f.Al_2O_3} \\
&- 5X_{Fe}X_{Ni}{}^0\Omega_{Fe-Ni} - 10X_{Fe}X_{Ni}(X_{Fe} - X_{Ni})^1\Omega_{Fe-Ni} \\
&+ X_{Fe}(2 - 5X_{Al})^0\Omega_{Fe-Al} + X_{Fe}(2X_{Fe} - 4X_{Al} \\
&- 10X_{Fe}X_{Al} + 10X_{Al}^2)^1\Omega_{Fe-Al} \\
&+ X_{Fe}(3 - 5X_O)^0\Omega_{Fe-O} + X_{Fe}(3X_{Fe} - 6X_O \\
&- 10X_{Fe}X_O + 10X_O^2)^1\Omega_{Fe-O} \\
&+ X_{Ni}(2 - 5X_{Al})^0\Omega_{Ni-Al} + X_{Ni}(2X_{Ni} \\
&- 4X_{Al} - 10X_{Ni}X_{Al} + 10X_{Al}^2)^1\Omega_{Ni-Al} \\
&+ X_{Ni}(X_{Ni} - X_{Al})(2X_{Ni} - 6X_{Al} - 15X_{Ni}X_{Al} \\
&+ 15X_{Al}^2)^2\Omega_{Ni-Al} + X_{Ni}(3 - 5X_O)^0\Omega_{Ni-O} \\
&+ X_{Ni}(3X_{Ni} - 6X_O - 10X_{Ni}X_O - 10X_O^2)^1\Omega_{Ni-O} \\
= &-(3X_{Al} + 2X_O - 5X_{Al}X_O)^0\Omega_{Al-O}
\end{aligned} \tag{27}
$$

Taking Y_{Al-O} on the vertical axis and $-(3X_{Al}+2X_O-5X_{Al}X_O)$ on the horizontal axis, $^0\Omega_{Al-O}$ was obtained as the slope of the regression line through multiple Y_{Al-O} and $-(3X_{Al}+2X_O-5X_{Al}X_O)$ data points
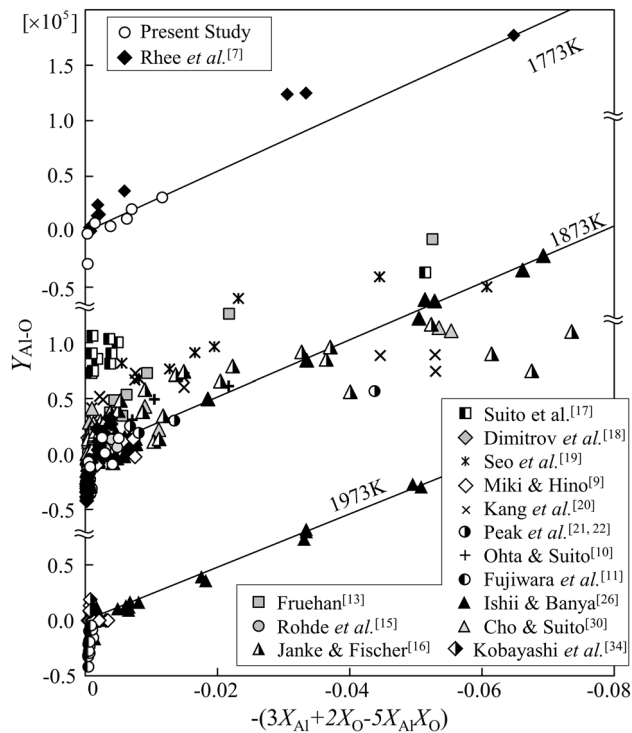
Fig. 8—Determination of the Al-O interaction parameter.

Table III. Lists of Thermodynamic Data from Literature and Those Determined in this Study

	Values [J]	Ref.
$^{0}\Omega_{Fe\text{-}Ni}$	$-16911 + 5.1622T$	28
$^{1}\Omega_{Fe\text{-}Ni}$	$10180 - 4.146656T$	28
$^{0}\Omega_{Fe\text{-}Al}$	$-291670 + 117.4T$	present study
$^{1}\Omega_{Fe\text{-}Al}$	$85260 - 39.36T$	present study
$^{0}\Omega_{Fe\text{-}O}$	$-415400 + 142.4T$	29
$^{1}\Omega_{Fe\text{-}O}$	$298300 - 117.8T$	29
$^{0}\Omega_{Ni\text{-}Al}$	$-97200 + 30.0T$	present study
$^{1}\Omega_{Ni\text{-}Al}$	$-301800 + 40.5T$	present study
$^{2}\Omega_{Ni\text{-}Al}$	$-62900 + 104.5T$	present study
$^{0}\Omega_{Ni\text{-}O}$	$-106500 + 44.80T$	29
$^{1}\Omega_{Ni\text{-}O}$	$35500 - 15.92T$	29
$^{0}\Omega_{Al\text{-}O}$	$-5626500 + 1635T$	present study
$\Delta G^{\circ}_{Al_2O_3}$	$-1682300 + 324.15T$	27

calculated from the Al deoxidation equilibirum in Fe[13,15–22,34], Ni[26] and Fe-Ni alloy[7,9–11,30] in Figure 8. Compared with the previous Al-O interaction parameter[9] determined only from the data of Fe, the newly determined Al-O interaction in this study (Eq. [28]) is believed to be more reliable as the parameter ($^{0}\Omega_{Al\text{-}O}$) was determined from comprehensive experimental data of Fe, Ni and Fe-Ni alloy.

$$^{0}\Omega_{Al-O} = -5626500 + 1635T \qquad [28]$$

3. Al-O correlation

By using the newly determined interaction parameters of Fe-Al, Ni-Al and Al-O in this work, the Al-O correlation of the Al deoxidation equilibrium in Fe-Ni alloy can be thermodynamically predicted by Miki and
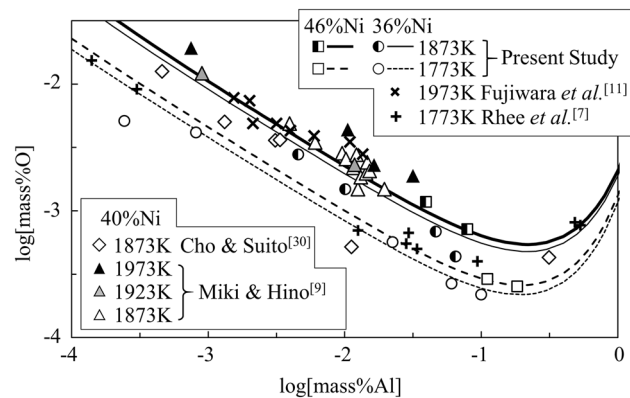

Fig. 9—Calculation of Al deoxidation equilibrium in Fe-36 to 46 pct Ni.
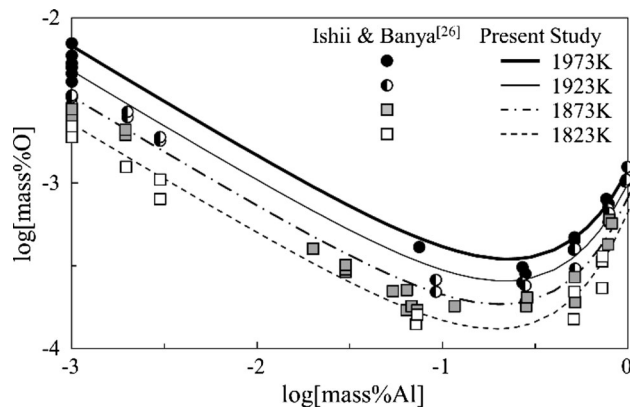

Fig. 10—Calculation of Al deoxidation equilibrium in Ni at 1823 K to 1973 K.

Hino's formula considering the third-order interaction parameters of Ni-Al (i.e., Eq. [15]). The interaction parameters and Gibbs free energy of Al_2O_3 formation ($\Delta G^{\circ}_{f.Al_2O_3}$) employed for the Al-O equilibrium calculation in this study are summarized in Table III. The calculated results of the Al-O correlation in the Al deoxidation equilibrium are shown in Figure 4 (Fe at 1873 K), Figure 9 (Fe-36 to 46 mass pct Ni alloy at 1773 K and 1873 K) and Figure 10 (Ni at 1773 K to 1973 K), respectively. For Fe (Figure 4), the present calculation on Al-O equilibrium correlation is similar to that of Miki and Hino[9] and is in a good agreement with the experimental data in the low Al region (Al < 0.5 mass pct), where the liquid metal can be considered as a regular solution. As shown in Figure 9, for the Al deoxidation equilibrium in Fe-36 to 46 mass pct Ni the present calculation agrees well with the measured result even in the low oxygen region. This confirms that the dissolved oxygen determination (in this work) by combination of the total oxygen measurement and inclusion analysis is not only precise but also reliable. It is clear that in Figure 10, the Al deoxidation equilibrium in Ni is precisely calculated by using the parameters determined in this study. As compared to
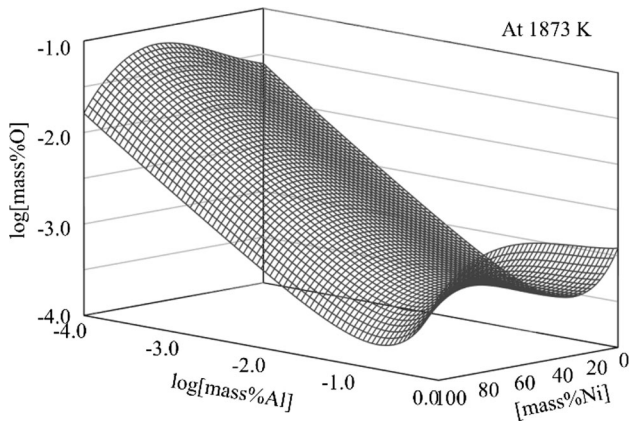
Fig. 11—Calculation of Al deoxidation equilibrium in Fe-Ni alloy at 1873 K.

Figure 5, it is notable that the newly determined parameters in this study greatly improved the calculation validity in the high Ni region (see Figure 10). Figure 11 shows as an example the Al-O correlation of the deoxidation equilibrium in the complete composition range of Fe-Ni alloys at 1873 K. By using the parameters in Table III and Eq. [15], the Al-O correlation in the temperature range of 1773 K to 1973 K can be predicted. Although the parameters obtained in this article are valid for Fe-Ni alloys over the entire composition range of Fe and Ni but only in the dilute region of O and Al, these parameters will help us to describe the Al deoxidation reactions during solidification of large ingots, thereby enabling the quality control of the casted ingots.

IV. CONCLUSION

The Al deoxidation equilibrium in molten Fe-Ni alloy was experimentally determined at 1773 K and 1873 K. The dissolved oxygen in the metal samples was determined from the total oxygen content (LECO) and the undissolved oxygen content determined from SEM-EDS inclusion analysis. The Al deoxidation equilibrium was expressed by using the Redlich–Kister type polynomial with up to the third-order interaction parameters of Ni-Al. The interaction parameters were determined by the measured deoxidation product in the complete composition range of Fe-Ni alloys from 1773 K to 1973 K.

$$^{0}\Omega_{\text{Fe-Al}} = -291670 + 117.4T$$

$$^{1}\Omega_{\text{Fe-Al}} = 85260 - 39.36T$$

$$^{0}\Omega_{\text{Ni-Al}} = -97200 + 30.0T$$

$$^{1}\Omega_{\text{Ni-Al}} = -301800 + 40.5T$$

$$^{2}\Omega_{\text{Ni-Al}} = -62900 + 104.5T$$

$$^{0}\Omega_{\text{Al-O}} = -5626500 + 1635T$$

$$(1773K \leq T \leq 1973K, 0 \leq X_{\text{Al}} \leq 0.02)$$

By using the interaction parameters obtained in this work, the Al deoxidation equilibrium can be described with high accuracy in the complete composition range of Fe-Ni alloys with dilute Al and O at temperatures from 1773 K to 1973 K.

REFERENCES

1. C. Wagner: *Thermodynamics of Alloys*, Addison-Wesley Press, Cambridge, MA, 1952, pp. 47–51.
2. T. Miki and M. Hino: *ISIJ Int*., 2004, vol. 44, pp. 1800–09.
3. L.S. Darken: *Trans. Met. Soc. AIME*, 1967, vol. 239, pp. 80–89.
4. L.S. Darken: *Trans. Met. Soc. AIME*, 1967, vol. 239, pp. 90–96.
5. M. Hillert and L.-I. Staffanson: *Acta Chem. Scand*., 1970, vol. 24, pp. 3618–26.
6. N. Saunders and A.P. Miodownik: *Calphad (Calculation of Phase Diagrams), A Comprehensive Guide*, Pergamon, Oxford, 1988, pp. 92–97.
7. S.B. Lee, S.M. Jung, H.G. Lee, and C.H. Rhee: *ISIJ Int*., 2002, vol. 42, pp. 679–84.
8. R.T. DeHoff and F.N. Rhines: *Quantitative Microscopy*, McGraw-Hill Publishing Co., Ltd., New York, 1968.
9. A. Hayashi, T. Uenishi, H. Kandori T. Miki M. Hino: *ISIJ Int*., 2008, vol. 48, pp. 1533–41.
10. H. Ohta and H. Suito: *ISIJ Int*., 2003, vol. 43, pp. 1301–08.
11. H. Fujiwara, A. Hattori, and E. Ichise: *Tetsu-to-Hagané*, 1999, vol. 85, pp. 201–07.
12. D.C. Hilty and W. Crafts: *J. Met*., 1950, vol. 2, pp. 414–24.
13. R.J. Fruehan: *Metall. Trans*., 1970, vol. 1, pp. 3403–10.
14. H. Schenck, E. Steinmetz, and K.K. Mehta: *Arch. Eisenhüttenwes*., 1970, vol. 41, pp. 131–38.
15. L.E. Rohde, A. Choudhury, and M. Wahlster: *Arch. Eisenhüttenwes*., 1971, vol. 42, pp. 165–74.
16. D. Janke and W.A. Fischer: *Arch. Eisenhüttenwes*., 1975, vol. 46, pp. 297–302.
17. H. Suito, H. Inoue, and R. Inoue: *ISIJ. Int*., 1991, vol. 31, pp. 1381–88.
18. S. Dimirov, A. Weyl, and D. Janke: *Steel Res*., 1995, vol. 66, pp. 3–7.
19. J.D. Seo, S.H. Kim, and K.R. Lee: *Steel Res*., 1998, vol. 69, p. 4953.
20. Y. Kang, M. Thunman, D. Sichen, T. Morohoshi, K. Mizukami, and K. Morita: *ISIJ Int*., 2009, vol. 49, pp. 1483–89.
21. M.K. Paek, J.M. Jang, Y.B. Kang, and J.J. Pak: *Metall. Mater. Trans. B*., 2015, vol. 46B, pp. 1826–36.
22. M.K. Paek, J.J. Pak, and Y.B. Kang: *Metall. Mater. Trans. B*., 2015, vol. 46B, pp. 2224–32.
23. The Japan Society for Promotion of Science The 19th Committee in Steelmaking: *Steelmaking Data Sourcebook*, Gordon and Breach Science Publishers, New York, 1988.
24. H. Itoh, M. Hino, and S. Ban-ya: *Tetsu-to-Hagane*, 1997, vol. 83, pp. 773–78.
25. I.H. Jung, S.A. Decterov, and A.D. Pelton: *Metall. Mater. Trans. B*, 2004, vol. 35B, pp. 493–507.
26. F. Ishii, S. Ban-ya, and M. Hino: *ISIJ Int*., 1996, vol. 36, pp. 25–31.
27. M.W. Chase, Jr.: *NIST-JANAF Thermochemical Tables*, 4th ed., AIP, Woodbury, NY, 1998.
28. B.J. Lee: *CALPHAD*, 17(1993), vol. 17, pp. 251–68.

29. T. Miki and M. Hino: *ISIJ Int.*, 2005, vol. 45, pp. 1848–55.
30. S.W. Cho and H. Suito: *Steel Res.*, 1995, vol. 66, pp. 237–43.
31. A.K. Niessen, F.R. de Boer, R. Boom, P.F. de Châtel, W.C.M. Matterns, and A.R. Miedema: *CALPHAD*, 1983, vol. 7, pp. 51–70.
32. G.K. Sigworth, J.F. Elliot, G. Vaughn, G.H. Geiger *et al.*: *Trans. Met. Soc. CIM,* Annual Volume 1977, pp. 104–10.
33. V.G. Dyubanov, A.Y. Stomakhin, and A.F. Filippov; *Izv. V. U. Z. Chernaya Metall.*, 1972, No. 3, pp. 69–71.
34. K. Kobayashi, Y. Omori, and K. Sanbongi: *Tetsu-to-Hagané*, 1967, vol. 53, pp. 141–44.